Designing Polymer Thick Film Intracranial Electrodes for Use in Intra-Operative MRI Setting.

G. Bonmassar[1]* and A. Golby[2]

[1]AA. Martinos Center, Massachusetts General Hospital, [2]Departments of Neurosurgery and Radiology, Brigham and Women's Hospital.

*Corresponding author: Giorgio Bonmassar, Building 149, 13th Street, M.S.: 2304, Charlestown, MA 02129, email address: giorgio@nmr.mgh.harvard.edu

Abstract: A new type of MRI compatible intracranial electrode based on Polymer Thick Film (PTF) is presented and studied using COMSOL Multiphysiscs. The geometry considered was a two-dimensional cross section cut of 5 mm thick electrodes with 5 cm leads on top of a 2×10 cm slab representing Gelfilm, or the substrate. The resistive leads were compared with metallic leads to estimate the Faradays induced current density noise. When free electrons in the leads are exposed to Lorentz forces due to the motion of the leads in the static magnetic field $\mathbf{B_0}$ the resulting induced current is named ballistocardiogram noise due to its cardiac motion component. In metallic materials the carrier density is very high (10^{22} electrons/cm^{-3}) compared to resistive leads. The results show that PTF resistive leads may reduce by up to three orders of magnitude the ballistocardiogram-induced current densities of the leads.

Keywords: Ballistocardiogram, Faraday's Law, and magnetoquasistatic (MQS) approximation.

1. Introduction

The use of intra-operative MRI-guidance during surgery for brain tumors provides the surgeon with a powerful tool to define the structural anatomy of the patient's brain and tumor and can help to maximize resection of the tumor. Knowledge about the patient's functional anatomy may be acquired through subdural electrocortical recordings and stimulation. Electrocortical recording in the MRI environment could be an important adjunct when operating in or near functionally important brain areas in order to avoid causing a neurologic deficit. However, artifacts introduced by the static magnetic field in both the electrophysiological and MRI signals have prevented the use of such techniques in MRI-guided surgeries (**Fig. 1**). In subdural recordings there is pulsativity of the brain surface that produces artifacts. Similarly in the more common EEG/MRI recordings, this noise is named "ballistocardiogram noise". The ballistocardiogram (BCG) has been recognized for over 50 years: it is produced when blood from the heart is pumped upwards along the ascending aorta. When the heart pumps blood, the major motion is along the axis parallel to the spine as a rocking movement of the patient's body at each heart beat [1]. This type of noise is of small amplitude, is not present in every subject, and is easy to eliminate outside of the MRI environment by using damping foam or by placing the subject in a position other than supine during EEG recordings. The first EEG recordings obtained inside MRI scanners were also characterized by pulse related noise [2]; this was interpreted as being due to pulsatile whole-body, head or scalp motion, time locked to the cardiac cycle [3-5].

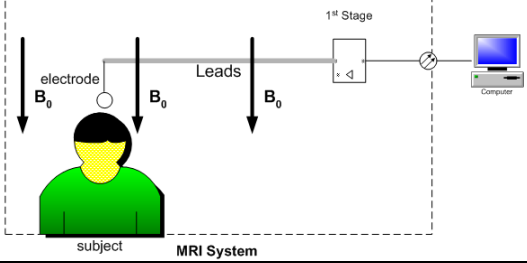

Fig. 1. *Electrophysiology in an intraoperative MRI unit.*

The Ballistocardiogram noise can be sharply reduced by changing the dielectric properties of the leads [6]. In this study we use FEMLAB to estimate the dielectric properties for the intracranial/subdural electrodes for use in the intra-operative setting for MRI recordings. The proposed electrodes will be constructed by

depositing Polymer Thick Film with the resulting dielectric properties on top of absorbable gelatin film (i.e., Gelfilm by Pharmacia and Upjohn Co, Division of Pfizer Inc, NY), which is commonly used in neurosurgery to separate the dura from the overlying soft tissue when the cranial bone needs to be removed. The proposed electrode set has the potential to greatly advance patient monitoring during image-guided surgery for brain tumors.

2. The Theory.

The case of a conductive object Ω moving with a small velocity **v** inside a uniform magnetic field can be modeled using the quasi-static fields approximation or that the dimensions of the object is small compared to the wavelength. The use of magnetoquasistatic (MQS) is justified since we neglect the presence of displacement currents (i.e., $\partial \mathbf{D}/\partial t = 0$) and $f_0^2 \mu_0 \varepsilon_0 L^2 << 1$, where L is the maximum dimension of the object under Ω consideration and f_0 is the frequency of Ω sinusoidal motion. The MQS approximation of the Maxwell equations is expressed in the following differential form:

$$\nabla \times \mathbf{E} = -\frac{\partial \mathbf{B}}{\partial t} \tag{1}$$

$$\nabla \times \mathbf{H} = \varepsilon_0 \frac{\partial \mathbf{E}}{\partial t} + \mathbf{J} \cong \mathbf{J} \tag{2}$$

$$\nabla \cdot \mathbf{E} = \frac{\rho}{\varepsilon_0} \tag{3}$$

$$\nabla \cdot \mathbf{H} = 0 \tag{4}$$

From the basic macroscopic properties of the material:

$$\mathbf{B} = \mu_0 (\mathbf{H} + \mathbf{M}) \tag{5}$$

$$\mathbf{J} = \sigma (\mathbf{E} + \mathbf{v} \times \mathbf{B}) \tag{6}$$

$$\mathbf{E} = -\Delta V - \frac{\partial \mathbf{A}}{\partial t} \tag{7}$$

The following Lorentz force expresses the force acting on a single charge in a magnetic field $\mathbf{B_0}$ with a velocity **v**:

$$\mathbf{F}_l = q\mathbf{v} \times \mathbf{B} \tag{8}$$

since the force acting on a single charge by electric field is $\mathbf{F}_e = q\mathbf{E}$, then the term $\mathbf{v} \times \mathbf{B}$ has the dimensions of an electric field and the term $\sigma \mathbf{v} \times \mathbf{B}$ in **eq.**(6) represent the currents induced in Ω by moving in constant velocity in a static magnetic field. In our case the velocity from **eq.**(2) and from the expression of the magnetic potential (i.e., $\mathbf{B} = \nabla \times \mathbf{A}$), we derive:

$$\nabla \times \left(\frac{1}{\mu_0} \nabla \times \mathbf{A} - \mathbf{M} \right) = \mathbf{J} \tag{9}$$

using **eq.**(6) and **eq.**(7), results:

$$\nabla \times \left(\frac{\nabla \times \mathbf{A}}{\mu_0 (1 + \chi_m)} \right) + \sigma \mathbf{v} \times (\nabla \times \mathbf{A}) + \sigma \frac{\partial \mathbf{A}}{\partial t} = \frac{\sigma \Delta V}{L} \tag{10}$$

The induced currents are modeled by the following expression of MQS under a null external potential (ΔV) and in cylindrical coordinates:

$$\sigma \frac{\partial A_\Phi}{\partial t} + \nabla \times \left(\frac{1}{\mu_0 \mu_r} (\nabla \times A_\Phi - \mathbf{B}_0) \right) + \sigma \mathbf{v} \times (\nabla \times A_\Phi) = 0 \tag{11}$$

Where A_Φ is the vector potential in the Φ-direction, μ_r is the material's relative permeability set 1, σ is the conductivity of the material, **v** is the velocity of the object Ω.

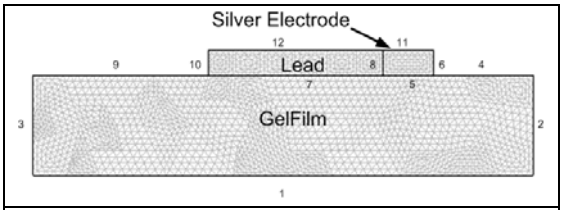

Fig. 2*: The geometrical model of the proposed electrodes is made of: (a) a Silver electrode tip ($\sigma_s = 6 \cdot 10^7$ S/m), (b) a lead ($\sigma_l = 1$ S/m) and (c) a Gelfilm substrate ($\sigma_{gf} = 1$ S/m). Numbers specify the boundary labels.*

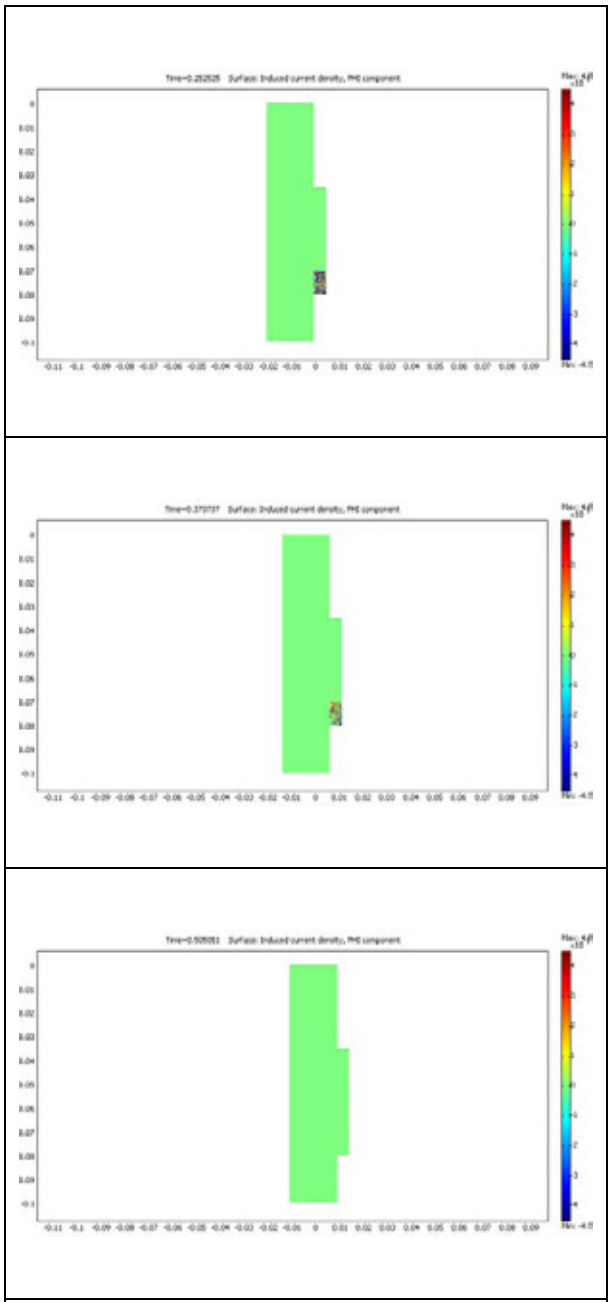

Fig. 3*: Cross-section of the PTF carbon (i.e.,* 119-28*) leads, current densities J_Φ in after 0 (top) 0.14 (middle) and 0.42 (bottom) seconds from onset of motion.*

3. The Geometric Model.

In ***Fig. 2*** is presented the geometrical model considered. A rectangle of 10×2cm represented the Gelfilm substrate, where the different types of PTF inks are laid. On top of this substrate a second rectangle 5mm×3.5cm represented the electrode lead that was a PTF either in silver (i.e., Ag) or in carbon (i.e., C). Finally the tip of the electrode was a rectangle 5mm×1cm in silver.

4. The Simulation Parameters.

The Finite Element Method (FEM) is being used to study the currents that are formed by Faraday induction, due to the movements of the leads inside the large magnetic field of the MRI bore. The simulations were performed in Multiphysiscs 3.2 (COMSOL, Burlington MA) using two 2D physical models: perpendicular induction currents (*emqa*) and moving mesh (*ale*).

The variables for the two models were: A_Φ (i.e., the magnetic potential in cylindrical coordinates) for *emqa*, and z (i.e., spatial coordinate in the direction of motion), r (i.e., constant spatial coordinate or motionless), lm2 and lm3 (i.e., lagrangian variables) for *ale*. The subdomain settings are defined by the properties of materials and the initial conditions for each model. **Table 1** describes the material properties and the product numbers refer to silver and carbon based PTF inks (Creative Materials Inc, Tyngsboro, MA). **Tables 2** and **3** the boundary settings for the two physical models are given. The boundary conditions around the perimeter of the geometry (**Fig.2**, *top left*), were set to $A_\Phi = 0$ (i.e., magnetic insulation).

The initial conditions were all null except for the $\mathbf{B}_0$ (i.e., the remnant external magnetic field or the static field of the MRI), which was set to 1 Tesla in the r-axis direction.

The scalar constants for *emqa* were the permittivity and permeability of vacuum: ε_0=8.854187817·10^{-12} F/m and $\mu_0 = 4\cdot\pi\cdot10^{-7}$ H/m.

The magnetoquasistatic (MQS) approximation of the Maxwell equations in **eq.**(11) was solved with the assumption that currents had only one nonzero component (i.e., 2D assumption). The displacement in *ale* was sinusoidal with excursion of ±10mm, a

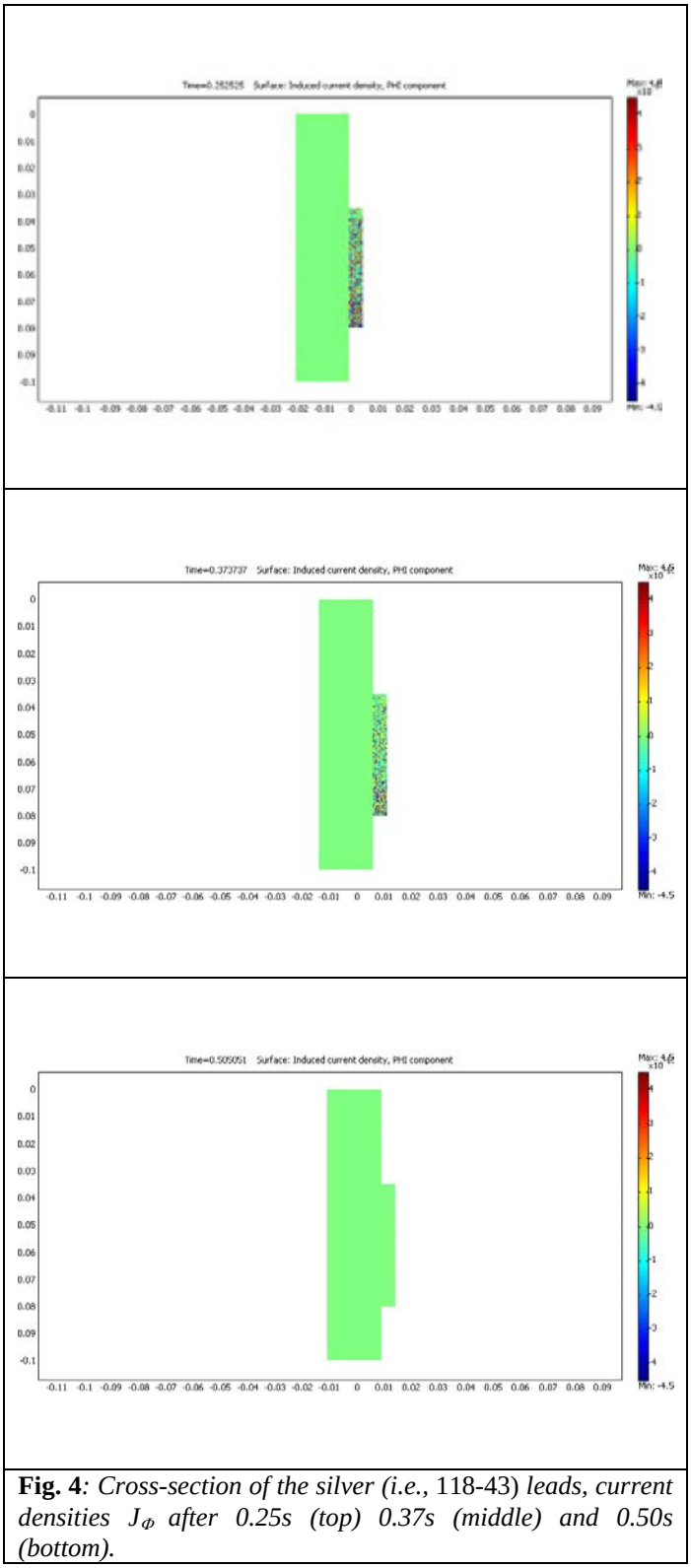

Fig. 4*: Cross-section of the silver (i.e.,* 118-43*) leads, current densities J_Φ after 0.25s (top) 0.37s (middle) and 0.50s (bottom).*

reasonable assumption of brain parenchymal motion with opening in the skull:

$$\Delta z = 0.01 \sin\left(\omega_0 \, t - \pi/2\right) \qquad (12)$$

where $\omega_0 = 2\pi$ or the frequency of the ballistocardiogram noise (i.e., main harmonic = 1 Hz), and $t = 0 \ldots 1\,\mathrm{s}$. The motion was directed perpendicular to $\mathbf{B_0}$ (r-direction) with a velocity in of:

$$v_z(t) = 0.01 \cdot \omega_0 \cos\left(\omega_0 \, t - \pi/2\right) \qquad (13)$$

Although, the velocity is not constant it can be approximately be considered constant if the simulation time step is small enough, the simulations were performed setting to `linspace(0,1,100)` the time stepping of the solver parameters. The eq.s (11) and (12) create the link between the two models: *ale* and *emqa*.

Finally, the mesh was a Delaunay set with a maximum element size of 10^{-4} m on all domains, and the adaptive refine meshing option, generating a mesh consisting of 38,100 elements and 76,701 DOF for the 2 models.

5. Results.

Fig. 3 shows the induced currents densities J_Φ with silver leads in time following the motion of the entire system (i.e., gelfilm, leads and electrodes), shown at three different time shots: after 0.25s (top) 0.37s (middle) and 0.50s. Only the silver tip has visible (i.e., colored) current densities. When t=0.25s the object is situated in its middle position, at t=0.50s the object is at the final 10mm shift the flux and induced currents are minimal. Quantitatively, the average current densities J_Φ (i.e., *JiPHI*) in the PTF carbon lead were: (t=0.25s) -7.3^{-19} A/m^2, (t=0.37s) $-3.6\cdot10^{-19}$ A/m^2 and (t=0. 0.505051s, reversed motion) $9.3\cdot10^{-20}$ A/m^2.

Similarly, **Fig. 4** shows the induced currents densities with silver leads in time following the motion of the entire system (i.e., gelfilm, leads and electrodes), shown at three different times: after 0.25s (top) 0.37s (middle) and 0.50s. This time the silver tip is not distinguishable from the silver lead (i.e., colored) current densities. This time, the average current densities J_Φ (i.e., *JiPHI*) in the silver PTF lead were: (t=0.25s) $4.3\cdot10^{-15}$ A/m^2, (t=0.37s) $3.7\cdot10^{-15}$ A/m^2 and (t=0.505051s) $5.7\cdot10^{-16}$ A/m^2.

The ratio between the silver induced currents and the resistive leads was at all times approximately 5,000; showing that the proposed new leads may have a rather substantial effect in reducing the motion induced currents and thus the noise that thus far has impeded our recordings on the surface of the patient's dura inside large magnetic fields.

MATERIAL	CONDUCTIVITY (S/m)	RELAT. PERMIT.	DENS. (Kg/m^3)
118-43	400	4.2	2,020
119-28	0.08	4.2	1,200
Gelfilm	0.33	10,000	8,700

Table 1: *Properties of materials.*

BOUNDARIES	VELOCITY (m/s)	WEAK CONSTR.	INTEGR. ORDER
1-4, 6-7, 9, 11	{0,1}	1	{1, 1}
5, 8, 10, 12	{0,0}	1	{1, 1}

Table 2: *Boundary settings for Moving Mesh.*

6. Conclusions.

The Finite Element simulations using the magnetoquasistatic (MQS) coupled with motion equations demonstrate that leads constructed with an intrinsic conductivity of less than 1 S/m, compared with the 400 S/m of the silver ink and 10^7 of traditional copper leads, may play a substantial role in reducing the Faraday motion induced noise signals.

The method is limited by the fact that the model is inherently two-dimensional, so we expect that in real measurements and in 3D the changes will be less than the ones shown by our 2D simulations.

BOUNDARIES	TYPE	RELAT. PERMIT	SURFACE IMPEDANCE (Ω)
1-4, 6, 9-12	Magnetic Insulation	1	1

Table 3: *Boundary settings for Perpendicular Induction Currents.*

7. References

1. *Reilly, J.P., Electrical stimulation and electropathology. 1992, New York: Cambridge Press.*
2. *Huang-Hellinger, F.R., et al., Simultaneous functional magnetic resonance imaging and electrophysiological recording. Human Brain Mapping, 1995. 3: p. 13-23.*
3. *Ives, J.R., et al., Monitoring the patient's EEG during echo planar MRI. Electroencephalography & Clinical Neurophysiology, 1993. 87(6): p. 417-420.*
4. *Nakamura, W., et al., Removal of ballistocardiogram artifacts from simultaneously recorded EEG and fMRI data using independent component analysis. IEEE Trans Biomed Eng, 2006. 53(7): p. 1294-308.*
5. *Schomer, D.L., et al., EEG-Linked functional magnetic resonance imaging in epilepsy and cognitive neurophysiology. J Clin Neurophysiol, 2000. 17(1): p. 43-58.*
6. *Vasios, C.E., et al. An Ink Cap for recording EEG during 7 Tesla MRI. in 11th Annual Meeting of the Organization for Human Brain Mapping. 2005. Toronto, Canada: Neuroimage.*
7. *Kamada, K., et al., Localization analysis of neuronal activities in benign rolandic epilepsy using magnetoencephalography. J Neurol Sci, 1998. 154(2): p. 164-72.*

8. Acknowledgements

The authors acknowledge the support of the Center for Integration of Medicine and Innovative Technology (CIMIT) and the NIH U41RR019703.

9. Electromagnetic Quantities

(a) The vector fields:

- **E:** Electric Field Strength (V/m)
- **B:** Magnetic Flux Density (Wb/m^2)
- **H:** Magnetic Field Strength (A/m)
- **D:** Electric Displacement (C/m^2)
- **J:** Electric Current Density (A/m^2)
- **A:** Magnetic Potential (V s/m)
- **M:** Magnetization (A/m)
- **v**: Velocity (m/s)
- $\mathbf{F}_l$: Lorentz Force (N)

$\mathbf{F}_e$: Electric Force (N)

(b) The scalar fields:

ρ: Electric Charge Density (C/m^3)
V: Electric Potential (V)

(c) The scalar variables:

ε_0: Permittivity of Vacuum (F/m)
μ_0: Permeability of Vacuum (H/m)
μ_r: Permeability of material
σ_s: Conductivity of Electrode (S/m)
σ_l: Conductivity of Lead (S/m)
σ_{gf}: Conductivity of Lead (S/m)
ω_0: Ballistocardiogram angular frequency (rad/s)
f_0: Ballistocardiogram frequency (Hz)
L: Maximum dimension of object (m)
χ_m: Magnetic susceptibility
t: time (s)
q: test charge (C)